Journal of Biomolecular NMR, **17:** 203–214, 2000.
KLUWER/ESCOM

The relative orientation of the fibronectin ^{6}F1^{1}F2 module pair: A ^{15}N NMR relaxation study

Yasuhiro Hashimoto[a,b], Steven P. Smith[a], Andrew R. Pickford[a], Arnaud A. Bocquier[c], Iain D. Campbell[a] & Jörn M. Werner[a,*]
[a]*Department of Biochemistry, University of Oxford, South Parks Road, Oxford OX1 3QU, U.K.*
[b]*Analytical Research Laboratory, Asahi Chemical Industry, Co., Ltd., Shizuoka 416-8501, Japan*
[c]*Department of Structural Biology, Biomolecular Engineering Research Institute, Osaka 565-0874, Japan*

Received 23 February 2000; Accepted 18 April 2000

Key words: anisotropic diffusion, collagen-binding, fibronectin, module, ^{15}N relaxation

Abstract

The structure of a pair of modules (^{6}F1^{1}F2), that forms part of the collagen-binding region of fibronectin, is refined using heteronuclear relaxation data. A structure of the pair was previously derived from ^{1}H-^{1}H NOE and $^{3}J_{\mathrm{H}^{\alpha}\mathrm{HN}}$ data [Bocquier et al. (1999) *Structure*, **7**, 1451–1460] and a weak module–module interface, comprising Leu19 and Leu28, in ^{6}F1, and Tyr68 in ^{2}F1, was identified. In this study, the definition of the average relative orientation of the two modules is improved using the dependence of ^{15}N relaxation on rotational diffusion anisotropy. This structure refinement is based on the selection of a subset of structures from sets calculated with NOE and $^{3}J_{\mathrm{H}^{\alpha}\mathrm{HN}}$ data alone, using the quality of the fits to the relaxation data as the selection criterion. This simple approach is compared to a refinement strategy where ^{15}N relaxation data are included in the force field as additional restraints [Tjandra et al. (1997) *Nat. Struct. Biol.*, **4**, 443–449].

Introduction

Fibronectin is an extracellular glycoprotein, that exists both as a soluble dimer in plasma and as an insoluble component of the extracellular matrix (Hynes, 1990). It is involved in a number of important physiological events such as embryogenesis, wound healing, haemostasis and thrombosis. It is almost exclusively composed of three types of modules: F1, F2 and F3 (for a review, see Potts and Campbell, 1996). Combinations of the different modules allow fibronectin to present a variety of specific binding sites and functions that are distributed over the entire molecule. Different biological activities have been ascribed to different regions using a fragmentation approach.

Collagen plays an important role in the interaction between cells and extracellular matrix. Fibronectin binding to collagen has been localised to a 42 kDa region of fibronectin that is composed of the following six modules: ^{6}F1^{1}F2^{2}F2^{7}F1^{8}F1^{9}F1 (Hahn et al., 1979; Forastieri et al., 1985; Guidry et al., 1990). Attempts to further localise the binding region have given conflicting results. Gelatin (denatured collagen) binding affinity has been reported for the following fragments: ^{2}F2^{7}F1 (Owens et al., 1986; Litvinovich et al., 1991), ^{1}F2 and ^{1}F2^{2}F2 (Bányai et al., 1990), ^{6}F1^{1}F2 and ^{8}F1^{9}F1 (Ingham et al., 1989) and ^{6}F1^{1}F2^{2}F2^{7}F1 (Skorstengaard et al., 1994) with the ^{1}F2 module a key region of interaction (Bányai et al., 1991). A calorimetric study suggested that, within the collagen-binding region, ^{6}F1 and ^{7}F1 interact with each other (Litvinovich et al., 1991). Taken together, these observations suggest that the spatial arrangement of individual modules in the collagen-binding domain is crucial for the presentation of a collagen binding site. Since the structure determination of individual modules has elucidated potential interaction surfaces (Pickford et al., 1997), the study of larger fragments is

*To whom correspondence should be addressed. E-mail: jmw@bioch.ox.ac.uk

required to obtain information regarding their spatial arrangement.

The ^{6}F1^{1}F2 is the first module pair in the collagen-binding domain. The tertiary structure shown in Figure 1 has recently been determined by multi-dimensional NMR spectroscopy in our laboratory (Bocquier et al., 1999). While the structures of the individual modules ^{6}F1 and ^{1}F2 were well defined, only a small number of inter-module NOE restraints were obtained between Leu19 and Tyr68, and Leu28 and Tyr68, resulting in a large number of possible orientations of one module relative to the other.

Structure determination of macromolecules usually relies on the collection of close inter-proton distances (Wüthrich, 1986). However, in cases such as the ^{6}F1^{1}F2 module pair, where the macromolecule of interest consists of multiple domains with a limited number of observed inter-domain NOEs, the structure can be significantly underdetermined. This problem can be alleviated by using NMR parameters that depend on a global co-ordinate system and therefore provide relatively long-range structural information. Such approaches include the use of the dependence of ^{15}N relaxation on rotational diffusion anisotropy (Tjandra et al., 1997a), partial alignment of the molecules, caused either by an anisotropic magnetic susceptibility tensor (Tolman et al., 1995; Tjandra et al., 1997b) or by a magnetically oriented dilute liquid crystalline medium (Tjandra et al., 1997c).

Here we present the use of ^{15}N T_1 and T_2 relaxation to improve the definition of the relative orientation of the ^{6}F1^{1}F2 module pair. Two approaches were taken: one was a simple selection method where, from the family of structures calculated using only NOE and coupling constant restraints, a subset was selected on the basis of their fit to the relaxation data. In the other approach ^{15}N T_1/T_2 ratios were incorporated as harmonic restraints into the final structure refinement protocol (Tjandra et al., 1997a). In addition, the module–module interface was characterised by comparison of the backbone amide chemical shifts of ^{1}F2 in the presence and absence of the ^{6}F1 module.

Materials and methods

NMR data collection

The uniformly ^{15}N labelled ^{6}F1^{1}F2 module pair and ^{1}F2 single module were produced as described previously (Pickford et al., 1997; Bocquier et al., 1999). NMR measurements were carried out on 1.2 mM samples in H_2O/D_2O (95/5%) at pH 6.0. All spectra were collected at 298 K on a home-built spectrometer operating at 599.8 MHz (^{1}H frequency) using a triaxial gradient, triple-resonance probe. All experiments were recorded in a phase-sensitive manner using the States/TPPI method for quadrature detection in the indirectly detected dimensions (Marion et al., 1989).

Comparison of the ^{1}H and ^{15}N chemical shifts of the ^{1}F2 module in isolation and in the ^{6}F1^{1}F2 module pair was carried out with gradient enhanced ^{1}H-^{15}N HSQC spectra (Bodenhausen and Ruben, 1980; Kay et al., 1992a).

Two-dimensional {^{1}H}-^{15}N heteronuclear NOE experiments and a series of ^{1}H-^{15}N correlation spectra for the determination of ^{15}N T_1 and T_2 relaxation time constants were acquired using previously described methods incorporating pulsed field gradients for coherence pathway selection and water suppression (Kay et al., 1989, 1992a; Farrow et al., 1994). The acquisition times were 128.0 ms and 318.3 ms in t_2 (^{1}H) and t_1 (^{15}N), respectively. During the acquisition time the ^{15}N nuclei were decoupled with a 833 Hz GARP1 sequence (Shaka et al., 1985). ^{1}H saturation in the NOE experiment was effected by means of a train of 120° flip-angle pulses at 10-ms intervals for 3.5 s. Transverse relaxation time constants (T_2) were measured using a spin-echo sequence with a CPMG delay of 570 μs. Dipolar and chemical shift anisotropy (CSA) cross-correlation was removed by application of proton 180° pulses every 5 ms (T_1) and in the middle of the basic CPMG block (T_2) (Boyd et al., 1990; Kay et al., 1992b). Inaccuracies in T_2 measurements associated with sample heating were reduced by including a train of ^{15}N refocusing pulses and delays trailing the pulse sequence such that the total number of ^{15}N refocusing pulses was the same in each T_2 experiment (Wang and Bax, 1993). Heating was assessed by comparison of the NH chemical shift changes of T_2 spectra with the minimum and maximum number of ^{15}N refocusing pulses. The relaxation delays for T_1 and T_2 experiments were: T_1: 20 (twice), 80, 140, 220, 340, 500, 700, 1000 ms and T_2: 5.36 (twice), 16.08, 26.80, 42.88, 64.32, 96.48, 134.00, 187.60 ms.

The data were processed in FELIX 2.3 (Biosym, Inc., San Diego, CA, U.S.A.) with mild resolution enhancement in both dimensions. The longitudinal, T_1, and transverse, T_2, relaxation times were obtained by least-square fits of the resonance intensities to two-parameter exponential decays and the experimental errors were estimated from the standard deviations of the average intensity differences between repeated spec-

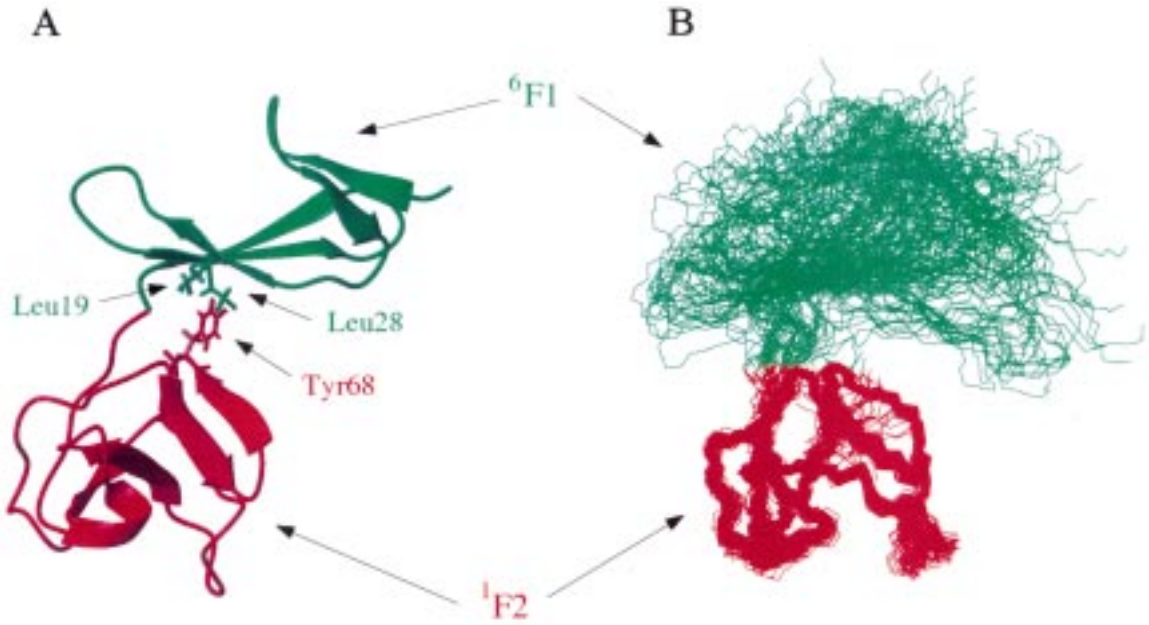

Figure 1. The structure of the ^{6}F1^{1}F2 module pair (Boquier et al., 1999). (A) Ribbon diagram of the average structure over the family of 55 calculated structures. The structure is characterised mainly by five β-strands in the ^{6}F1 and four in the ^{1}F2 module which assemble into anti-parallel β-sheets. (B) Overlay of the family of 55 structures when superimposed on the backbone heavy atom of the ^{1}F2 module. Although the structure of each module is well defined, there are relatively few inter-module NOEs so the relative module–module orientation is poorly defined. Figures were generated in MOLMOL 2.6 (Koradi et al., 1996).

tra (Palmer et al., 1991). The errors of the $\{^1H\}$-^{15}N heteronuclear NOE were approximated from Monte Carlo simulations using one standard deviation of baseline noise (J. Jones, personal communication).

Interpretation of relaxation data

The values of the ^{15}N-relaxation times were derived assuming dipolar and CSA relaxation using the usual fundamental constants and 1.02 Å as the NH bond length. The chemical shift anisotropy (CSA) was assumed to be -170 ppm and to be co-linear with the dipolar tensor (Tjandra et al., 1996). The principal axes D_x, D_y, D_z of the diffusion tensor D and its orientation (θ, ϕ, ψ) in the inertia frame were obtained by a global least-square fit of the spectral density functions of the T_1/T_2 ratios to the experimental values (Palmer et al., 1991; Mandel et al., 1995; Boyd and Redfield, 1998). Three models were tested: a sphere ($D_x = D_y = D_z$, $D = (D_x + D_y + D_z)/3$), a symmetric top ($D_\parallel = D_z$ and $D_\perp = (D_x + D_y)/2$), and a fully asymmetric tensor $D_x \neq D_y \neq D_z$ (Woessner, 1962). In the absence of chemical exchange, the spectral density of a symmetric top $J(\omega)$ is given by:

$$J(\omega) = \Sigma_{k=1,2,3}\, A_k[\tau_k/(1 + \omega^2\tau_k^2)] \qquad (1)$$

with

$$A_1 = (1.5\cos^2\theta - 0.5)^2 \quad A_2 = 3\sin^2\theta\cos^2\theta$$
$$A_3 = 0.75\sin^4\theta$$
$$\tau_1 = (6D_\perp)^{-1} \quad \tau_2 = (D_\parallel + 5D_\perp)^{-1}$$
$$\tau_3 = (4D_\parallel + 2D_\perp)^{-1}$$

where ω is the resonance frequency, and θ is the angle between the NH bond vector and the long axis, $D_\parallel$, of the diffusion tensor.

Estimation of the diffusion tensor and ranking of structures

The isotropic correlation time τ_m was estimated from an average T_1/T_2 value of the residues involved in the secondary structure within the range of one standard deviation. The residues used for the fitting were chosen carefully to exclude residues that are affected by either rapid or slow motion, or ones with ill-defined local structure, as indicated by low angular order parameters of the backbone dihedral angles. Eventually all the residues in secondary structure elements were used for fitting, except His3, Met16, Trp18, Asn63, Gly64 and Leu80. Subsequently, each of the 55 previously determined structures (Bocquier et al., 1999) was fit to the T_1/T_2 ratios using an axially symmetric and a fully asymmetric diffusion tensor with Modelfree4 (kindly

provided by A.G. Palmer III, Columbia University), and programs written in-house.

Once the appropriate diffusion model was established, the structures were ranked according to their χ^2 value as defined by

$$\chi^2 = \Sigma_i[\{(T_{1i}/T_{2i})_{\text{calc}} - (T_{1i}/T_{2i})_{\text{obs}}\}^2/\sigma_i^2] \quad (2)$$

where σ_i is the experimental uncertainty of the T_{1i}/T_{2i} ratio of each residue that was included. The 55 structures of the family were ranked according to their χ^2, and the best 15 structures (1st–15th with low χ^2), the medium structures (21st–35th with medium χ^2), and the poorest 15 structures (41st–55th with high χ^2) were selected and subjected to further analyses. Model comparisons were performed by using the *F*-test and calculation of the probability *Q* to obtain this *F* by chance (Press et al., 1990).

Structure refinement with T_1/T_2 restraints

Structure calculations were performed in X-PLOR v3.8 (Brünger, 1992) including the T_1/T_2 refinement routines (Tjandra et al., 1997a) kindly provided by Prof. M. Clore (NIH, Bethesda, MD), and statistical analysis of the structures was carried out using MOLMOL 2.6 (Koradi et al., 1996). Structure refinement with T_1/T_2 restraints was achieved by minimising the quadratic harmonic potential term E_{anis}:

$$E_{\text{anis}} = k_{\text{anis}}[(T_1/T_2)_{\text{calc}} - (T_1/T_2)_{\text{obs}}]^2 \quad (3)$$

where k_{anis} is a 'force constant', and $(T_1/T_2)_{\text{calc}}$ and $(T_1/T_2)_{\text{obs}}$ are the calculated and observed values of T_1/T_2, respectively (Tjandra et al., 1997a).

These T_1/T_2 restraints were incorporated into a refinement protocol, where 25 structures were refined with energy minimisation of E_{anis} in addition to the NOEs and dihedral angle restraints. The NOE force constant was 50 kcal/mol/Å^2 and the dihedral angle force constant 200 kcal/mol/rad^2. The temperature was decreased during the calculation (30 ps) from 1500 K to 100 K. A total of 15 refined structures was chosen on the basis of their low overall and E_{anis} energy.

Results and discussion

Chemical shift changes of the ^{1}F2 module in the presence of the ^{6}F1 module

Since the chemical shift is sensitive to local environment, changes in chemical shift are well suited to study even weak association phenomena. Figure 2 shows the ^{1}H-^{15}N HSQC spectra of the ^{6}F1^{1}F2 module pair and the ^{1}F2 single module and the difference of the amide ^{15}N and ^{1}H chemical shift of the ^{1}F2 module measured in isolation and in the ^{6}F1^{1}F2 module pair. Only a few residues show significant shift changes due to the presence of the ^{6}F1 module, confirming that the structure of the ^{1}F2 module is not significantly altered by the presence of ^{6}F1.

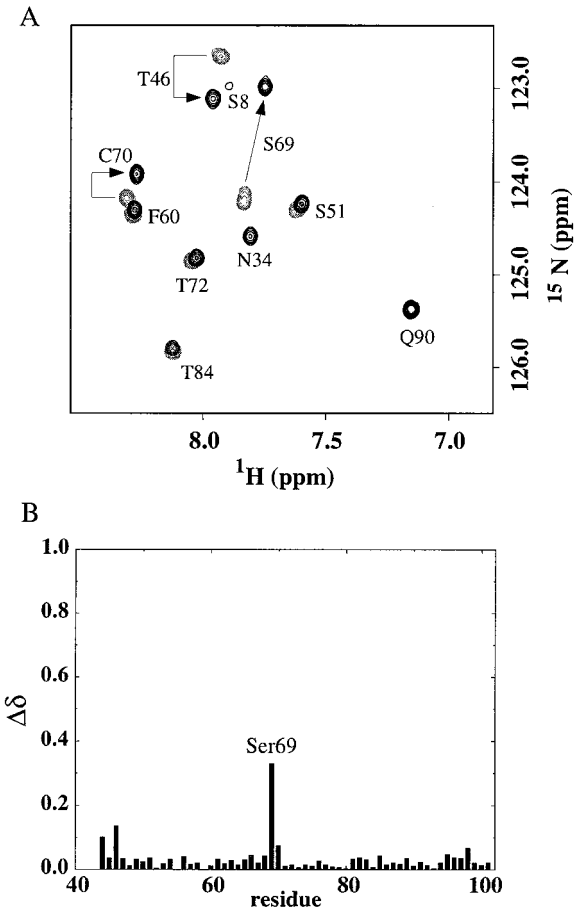

Figure 2. Amide ^{1}H and ^{15}N chemical shift changes of the ^{1}F2 module caused by the presence of the ^{6}F1 module. (A) A region of the ^{1}H-^{15}N HSQC spectra of the ^{6}F1^{1}F2 module pair (solid lines) as compared to the ^{1}F2 module in isolation (dotted lines). (B) The difference in chemical shift of the ^{1}F2 module in isolation and in the ^{6}F1^{1}F2 pair. Residue numbers correspond to those of the ^{6}F1^{1}F2 module pair. A single measure for the shift difference for each residue was obtained using the formula: $\Delta\delta = [(\Delta^1\text{H})^2 + (\gamma_N/\gamma_H)(\Delta^{15}\text{N})^2]^{1/2}$, where Δ^1H and Δ^{15}N are the observed proton and nitrogen chemical shift difference and γ_H and γ_N their respective gyromagnetic ratios.

The backbone amide ^{15}N and ^{1}H shifts of Ser69 are the only shifts that are significantly affected by the presence of the preceding ^{6}F1 module. In addition, the

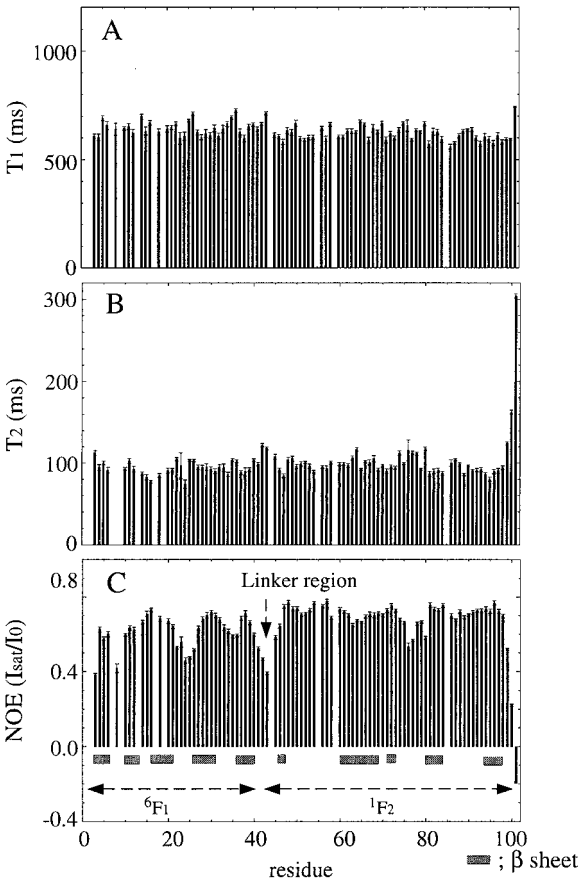

Figure 3. ^{15}N relaxation time constants of the ^{6}F1^{1}F2 module pair at 60.78 MHz and 298 K along the amino acid sequence. The positions of the β-strands are indicated by horizontal bars. (A) ^{15}N longitudinal (T_1) relaxation time constants. (B) ^{15}N transverse (T_2) relaxation time constants. (C) {^{1}H}-^{15}N NOE.

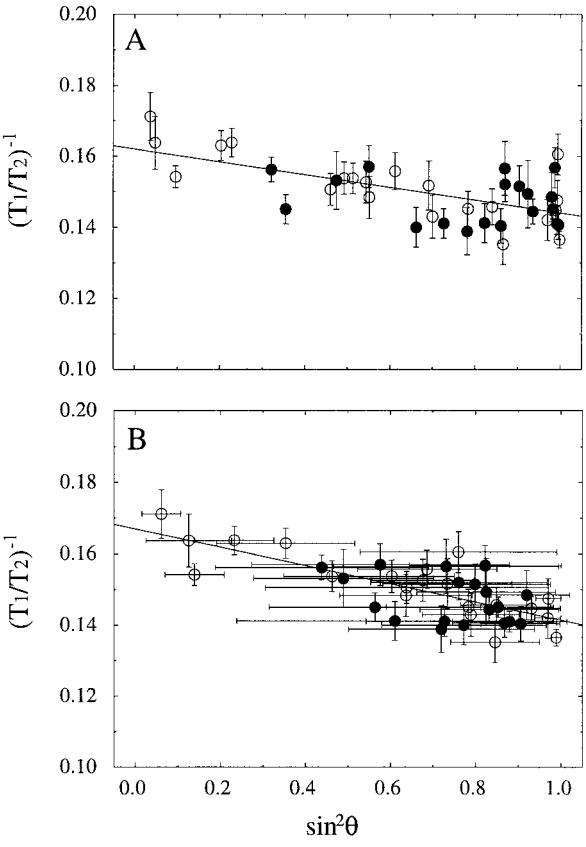

Figure 4. ^{15}N $(T_1/T_2)^{-1}$ ratios of individual residues as a function of the angle θ between the NH bond vector and the long axis of the diffusion tensor ($D_{\|}$). ^{6}F1 (filled circle) and ^{1}F2 (open circle). (A) Sin^2 θ for the average structure. (B) Average and standard deviation of $\sin^2$ θ for the family of 55 structures. The line represents a linear best fit to the data. The diffusion anisotropy $D_{\|}/D_{\perp}$ can be obtained from its slope (Copié et al., 1998).

H_2O exchange rate of the amide protons in the vicinity of Ser69 were reduced in the presence of the ^{6}F1 module (data not shown). Since Ser69 is located on the edge of a β-sheet in the isolated ^{1}F2 module, a local structural change is the probable explanation for the observed shift differences in the presence of the ^{6}F1 module. This is consistent with the observation of weak inter-module NOEs between Leu19, Leu28 in ^{6}F1 and Try68 in ^{1}F2 contributing to the inter-module interface (Bocquier et al., 1999).

^{15}N heteronuclear relaxation

The heteronuclear relaxation data are shown in Figure 3. The ^{15}N T_1, T_2 relaxation time constants in secondary structure regions have averages of 628.7 ms and 94.8 ms with average errors of 12.2 and 2.6 ms, respectively. The data show only small fluctuation for all residues, except Asp99–Thr101 in the C-terminus, which suggests that the modules are structured. This is confirmed by high average values (0.67) of the {^{1}H}–^{15}N NOE for residues in secondary structure elements. Smaller NOEs are observed for residues in the N- and C-termini and in the loop regions. Significantly reduced NOEs are seen for residues Thr41 to Glu45 in the linker between the ^{6}F1 and ^{1}F2 module, indicating the presence of sub-ns time scale motion for these residues. The lack of large chemical shift changes in the interface and the fast motion of the linker residues suggest some degree of flexibility between the modules. Comparison of the linker flexibility of module pairs from fibronectin shows that the ^{6}F1^{1}F2 pair falls into an intermediate range between the very flexible fibronectin ^{1}F1^{2}F1 pair without discernible preferential module–module orientation (Potts et al., 1999)

and the tight module–module association seen in the ^{4}F1^{5}F1 pair (Williams et al., 1994; Phan et al., 1996). Hence, the flexibility of the linker region appears to be correlated with the strength of the module–module association.

Estimation of the rotational diffusion tensor

To provide a quantitative analysis of the rotational diffusion properties of ^{6}F1^{1}F2, the relaxation data were fit to the family of 55 structures (Bocquier et al., 1999) assuming three different models: isotropic, axially symmetric and fully asymmetric tumbling (Table 1). A set of residues with well-defined NH bond vectors and T_1 and T_2 relaxation times dominated by the overall tumbling was chosen as described in Materials and methods. Fitting of the diffusion tensors was carried out using the data from the ^{6}F1 module, the ^{1}F2 module or the ^{6}F1^{1}F2 module pair (Table 1).

The isotropic correlation times of the individual modules and the pair are almost the same, suggesting that they can be analysed in a single diffusion frame. The analyses of the data from the individual modules indicate that the ^{6}F1^{1}F2 module has an oblate diffusion tensor. This is best shown by the low Q values of the oblate diffusion tensor for the ^{1}F2 module. Higher Q values are observed for the ^{6}F1 module with less significant improvements for any of the tested anisotropic models. The higher Q values are due to insufficient sampling of the NH bond vectors.

Using the data from both modules in the ^{6}F1^{1}F2 module pair, the axially symmetric and fully asymmetric models show significant improvement of the fitting compared to the isotropic model. Interestingly, two minima were found in the symmetric top model. One has an anisotropy of 1.14, corresponding to a prolate, the other 0.85, indicative of an oblate diffusion tensor. This underlines the importance to consider both models (Blackledge et al., 1998). No significant improvement was observed by further assuming an asymmetric model. This is in agreement with the observations that D_{xx} and D_{yy} exhibit similar values (1: 0.96 $\pm$ 0.03), and the anisotropy, $D_{\parallel}/D_{\perp}$ ($= 2\ D_{zz}/(D_{xx} + D_{yy})$), for both models was identical (0.85 ± 0.02). Since χ^2 was significantly lower in the oblate model than in the prolate (prolate: 2.51 ± 0.20, oblate: 1.78 ± 0.35), we concluded that the diffusion tensor of the molecule is an oblate.

Using the previously determined orientations of the diffusion tensors, the slope of $(T_1/T_2)^{-1}$ against $\sin^2\theta$ of the 55 structures (Copié et al., 1998), where θ is the angle between the NH bond vector and the main axis of diffusion tensor $D_{\parallel}$, yielded a diffusion anisotropy, $D_{\parallel}/D_{\perp}$, of 0.85, confirming that the molecule can be subjected to the T_1/T_2 analysis (Figure 4). Whereas almost all $(T_1/T_2)^{-1}$ of the averaged structure fall onto the theoretical line (Figure 4a), large deviations are observed for each residue for a significant number of structures from the family of 55 structures calculated on the basis of NOEs and coupling constants (Figure 4b). This indicates that, while the average structure agrees well with the ^{15}N relaxation time constants, the NOE-based family does not necessarily represent the most precise family of structures. Consequently, structure determination is expected to improve with inclusion of the ^{15}N relaxation restraints.

T_1/T_2 restraints in the structure determination

Selection method

Each member of the family of 55 structures (Bocquier et al., 1999) was fit to the experimental T_1/T_2 ratios assuming an axially symmetric diffusion tensor (oblate) and ranked according to the χ^2 of the relaxation data (see Materials and methods). Three classes were formed with 15 structures in each: the 'best' structures with lowest χ^2 (i.e. the structures whose calculated theoretical T_1/T_2 agreed best with experimental T_1/T_2), the 'medium' structures with intermediate χ^2, and the 'poorest' structures, with highest χ^2. Figure 5 shows the structures in each of the three classes superimposed on the ^{1}F2 module. The statistics of the structures, including χ^2 values and backbone RMSDs of the individual modules when overlaid on either of the three modules, are presented in Table 2. A significant improvement in the definition of the relative module–module orientation is observed, with an improved fit to the relaxation data, i.e. a decreasing χ^2 value. The subset of structures that agreed best with T_1/T_2 data (low χ^2) showed better precision of the average module–module orientation, as indicated by lower backbone RMSDs of 6.47 ± 2.89 (for the ^{1}F2 when superimposed on the ^{6}F1) and 6.19 ± 2.80 Å (for the ^{6}F1 when superimposed on the ^{1}F2), than the subset of the medium fit structures (intermediate χ^2) with values of 10.04 ± 5.04 and 9.64 ± 4.74 Å, and the poorest fit structures (high χ^2) with 11.03 ± 5.13 and 9.82 ± 4.56 Å. It is important to note that the structures in the three classes have comparable total energy, NOE violations and have similar percentages of residues in the allowed regions of the Ramachandran plot. This shows that the selection on the basis of

Table 1. Diffusion parameters for ^{6}F1^{1}F2 55 structures[†]

	$(6D)^{-1}$ (ns)	$2D_{zz}/(D_{xx}+D_{yy})$	$D_{xx} : D_{yy} : D_{zz}$	$\theta^{\ddagger}$	$\phi^{\ddagger}$	$\psi^{\ddagger}$	$\chi^2/N^{\$}$	$Q_1{}^{\#}$	$Q_2{}^{\#}$
Isotropic									
(a) ^{6}F1 ^{1}F2	7.61 ± 0.00	–	–	–	–	–	3.33 ± 0.0	–	–
(b) ^{6}F1	7.71 ± 0.00	–	–	–	–	–	1.79 ± 0.0	–	–
(c) ^{1}F2	7.58 ± 0.00	–	–	–	–	–	4.29 ± 0.0	–	–
Axially symmetric									
prolate[¶]									
(a) ^{6}F1 ^{1}F2	7.66 ± 0.02	1.14 ± 0.02	–	37.8 ± 21.4	134.9 ± 39.9	–	2.51 ± 0.20	1.7×10^{-4}	–
(b) ^{6}F1	7.78 ± 0.05	1.15 ± 0.05	–	67.1 ± 40.6	94.7 ± 54.0	–	1.33 ± 0.15	2.1×10^{-1}	–
(c) ^{1}F2	7.57 ± 0.02	1.20 ± 0.02	–	33.2 ± 17.2	152.9 ± 26.1	–	2.31 ± 0.24	1.5×10^{-3}	–
oblate[¶]									
(a) ^{6}F1 ^{1}F2	7.63 ± 0.03	0.85 ± 0.05	–	109.6 ± 22.9	108.5 ± 20.9	–	1.78 ± 0.35	1.1×10^{-10}	–
(b) ^{6}F1	7.68 ± 0.08	0.89 ± 0.03	–	104.6 ± 27.4	111.1 ± 33.2	–	1.26 ± 0.16	1.3×10^{-1}	–
(c) ^{1}F2	7.59 ± 0.01	0.83 ± 0.01	–	110.1 ± 6.1	118.2 ± 5.4	–	1.51 ± 0.20	8.3×10^{-6}	–
Asymmetric									
(a) ^{6}F1 ^{1}F2	7.64 ± 0.03	0.85 ± 0.02	$1 : 0.97\ (\pm 0.03) : 0.84\ (\pm 0.03)$	107.1 ± 10.5	110.3 ± 23.0	-25.0 ± 27.3	1.70 ± 0.34	–	8.0×10^{-1}
(b) ^{6}F1	N.D.	N.D.	N.D.	N.D.	N.D.	N.D.	N.D.	–	N.D.
(c) ^{1}F2	7.58 ± 0.01	0.83 ± 0.01	$1 : 0.94\ (\pm 0.02) : 0.81\ (\pm 0.01)$	113.7 ± 4.1	121.3 ± 4.6	-28.5 ± 12.5	1.33 ± 0.22	–	4.9×10^{-1}

[†]Parameters were obtained by fitting experimental T_1/T_2 values to the 55 structures calculated previously in our laboratory (Bocquier et al., 1999). Fits were carried out using the T_1/T_2 value of the residues in (a) both of the ^{6}F1 and ^{1}F2 modules, (b) the ^{6}F1 module and (c) the ^{1}F2 module.

[¶]A prolate ($2D_{zz}/(D_{xx}+D_{yy}) > 1.0$) or an oblate ($2D_{zz}/(D_{xx}+D_{yy}) < 1.0$) diffusion tensor was assumed. All values except Q_1 and Q_2 are given as averages and standard deviations of the family of 55 structures.

[‡]Euler angles of the principal axes of the diffusion tensor in the principal axis frame of the inertia tensor of the ^{1}F2 module.

[$]$\chi^2$ values per residue. N is the number of residues used for fits. N = (a) 40, (b) 19 and (c) 21.

[#]Q_1 was calculated for the comparison of the isotropic and axially symmetric models. The value given is the largest value of 66% of all structures. Q_2 was calculated for the comparison of the axially symmetric (oblate) and asymmetric models. The value given is the smallest value of 66% of all structures. Note that the maximum Q_1 of 90% were 2.2×10^{-3} (^{6}F1^{1}F2: prolate), 6.5×10^{-1} (^{6}F1: prolate), 5.1×10^{-3} (^{1}F2: prolate), 1.2×10^{-7} (^{6}F1^{1}F2: oblate), 3.6×10^{-1} (^{6}F1: oblate) and 3.9×10^{-5} (^{1}F2: oblate). The minimum Q_2 of 90% were 4.0×10^{-2} (^{6}F1 ^{1}F2) and 1.5×10^{-1} (^{1}F2).

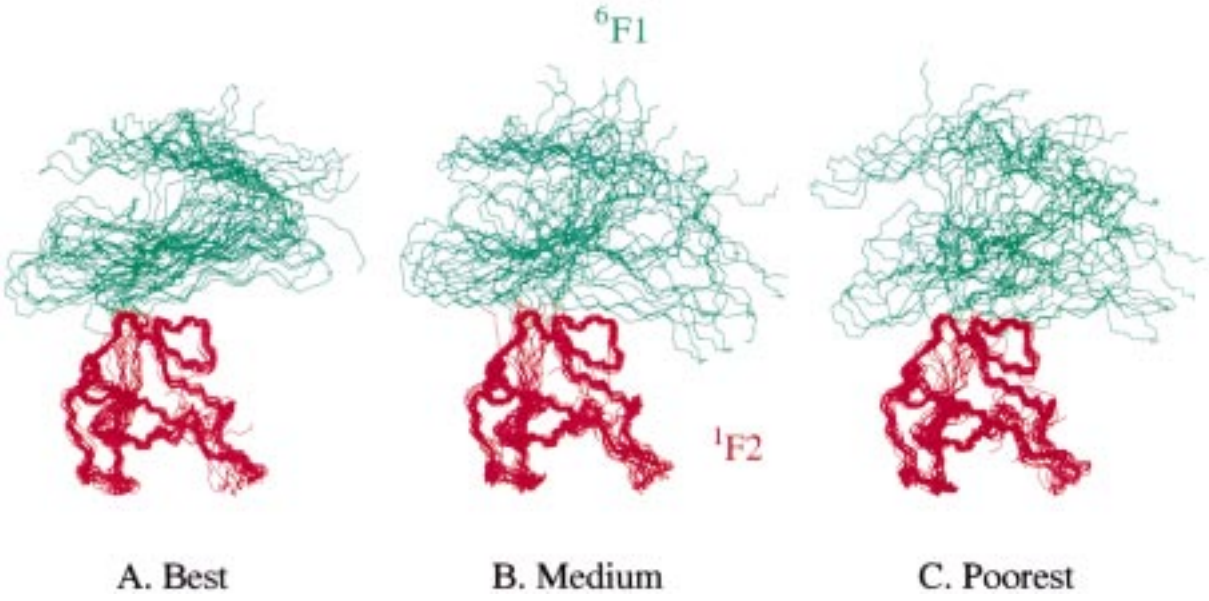

Figure 5. Selection of structures according to their agreement with the experimental T_1/T_2 ratios. Each subset contains 15 ^{6}F1^{1}F2 structures that are superimposed on the backbone heavy atoms of the ^{1}F2 module. (A) Structures that agreed best with the experimental T_1/T_2 ratios (low χ^2). (B) Structures with an intermediate χ^2. (C) Structures that agreed least with the experimental T_1/T_2 (high χ^2).

Table 2. Statistic of structures selected by fitting T_1/T_2*

	A (best)	B (medium)	C (poorest)
χ^2/N$	1.41 ± 0.10	1.71 ± 0.05	2.17 ± 0.28
RMSD (Å)†			
(a)	6.47 ± 2.89	10.04 ± 5.04	11.03 ± 5.13
(b)	1.35 ± 0.30	1.33 ± 0.35	1.33 ± 0.35
(c)	6.19 ± 2.80	9.64 ± 4.74	9.82 ± 4.56
(d)	1.19 ± 0.27	1.27 ± 0.34	1.17 ± 0.26
X-PLOR potential energies‡	58.95 ± 8.03	57.73 ± 6.68	58.39 ± 11.72
NOE violations¶			
> 0.3 Å	0	0	0
> 0.1 Å	2.9 ± 2.8	2.8 ± 1.5	2.7 ± 3.2
Structure quality#			
% residues in generously allowed region of Ramachandran plot	90.6	91.5	92.4

*Averages and standard deviations of 15 structures are given.
$$\chi^2$ values per residue ($N = 40$).
†Four RMSD values are calculated for each group: Backbone RMSD of (a) the ^{1}F2 module and (b) the ^{6}F1 module when overlaid with the ^{6}F1 moiety. RMSD of (c) the ^{6}F1 module and (d) the ^{1}F2 module when superimposed with the ^{1}F2 moiety.
‡Total potential energy in kcal/mol.
¶Average numbers of violations per structure and standard deviations.
#The program PROCHECK (Laskowski et al., 1993) was used to check the quality of the structures.

Table 3. Statistics of refined structures with or without T_1/T_2*

	A (with T_1/T_2)	B (without T_1/T_2)
χ^2/N$	1.42 ± 0.15	1.80 ± 0.27
RMSD (Å)†		
(a)	6.84 ± 3.79	9.82 ± 4.78
(b)	1.24 ± 0.30	1.13 ± 0.33
(c)	6.64 ± 3.81	9.27 ± 4.51
(d)	1.20 ± 0.30	1.18 ± 0.30
X-PLOR potential energies‡	64.36 ± 8.24	53.06 ± 5.34
NOE violations¶		
> 0.3 Å	0	0
> 0.1 Å	2.0 ± 1.7	1.3 ± 1.3
Structure quality#		
% residues in generously allowed region of Ramachandran plot	91.2	90.8

*$†‡¶#The indications are identical with Table 2.

T_1/T_2 ratios provides genuinely new information about the module–module interface.

T_1/T_2 refinement

In the second approach, the T_1/T_2 ratios were incorporated as additional restraints during the refinement stage of the structure calculation. All the calculations started from structures that were calculated using only NOEs and coupling constants (Bocquier et al., 1999). The quality of the refined structures was assessed by their total energy, the number of NOE violations, and the definition of local structure. The agreement with the T_1/T_2 ratios was measured by the χ^2 of the data. The definition of the module–module orientation was evaluated by comparing the RMSDs of the individual modules when superimposed on the respective partner.

Establishing the parameters for the refinement

Since the appropriate force constants for the restraint potentials of the T_1/T_2 ratios are not known a priori, they have to be determined for each molecule. In some molecules, insufficient sampling of the angles in the diffusion frame means that the diffusion tensor is relatively ill-defined. Hence, the relevant parameters have to be sampled and optimised for each molecule by a systematic search of the parameter space.

In the refinement of the ^{6}F1^{1}F2 module pair, $D_\parallel/D_\perp$ was optimised first using a force constant of 0.5–1.0 kcal/mol. The initial value of 0.85 was obtained by the T_1/T_2 fitting to the family of 55 structures (Table 1). However, as was noted earlier, the probability of finding an NH vector that is aligned with the $D_\parallel$ is small, and the minimum experimental T_1/T_2 value (in the case for an oblate) may therefore not be realised (Tjandra et al., 1997a). In a search for an optimum value $D_\parallel/D_\perp$ was thus varied (0.90, 0.85, 0.8 and 0.7). Better definition of relative module orientation was achieved for every value of $D_\parallel/D_\perp$ (backbone RMSD: approximately 6–7 Å for one module when superimposed on the other module) compared to the family of structures calculated without T_1/T_2 restraints, which exhibits a large range of orientation with backbone RMSDs of 9.82 ± 4.78 (for the ^{1}F2 when superimposed on the ^{6}F1) and 9.27 ± 4.51 Å (for the ^{6}F1 when superimposed on the ^{1}F2). Decreasing the value for $D_\parallel/D_\perp$ to below 0.8 resulted in structures with high total and E_{anis} energy, and a larger number of NOE violations. Thus the values of 0.85 and 0.90 were deemed to be optimal.

In the second step, the force constant was optimised by varying its value from 0.5 to 10 kcal/mol in a series of structure refinements. The results were monitored using χ^2 of the T_1/T_2 ratios, total energy, and the number of NOE violations in the structures. As expected, larger force constants resulted in the lower χ^2 values. For instance, a force constant of 10 kcal/mol decreased the χ^2 per residue to as low as 1.0. However, the total energy of the structures increased significantly to over 100 kcal/mol. In this study, a force constant that was linearly raised from 2.0 to 3.0 kcal/mol during the refinement was chosen because it yielded the best overall results (Table 3).

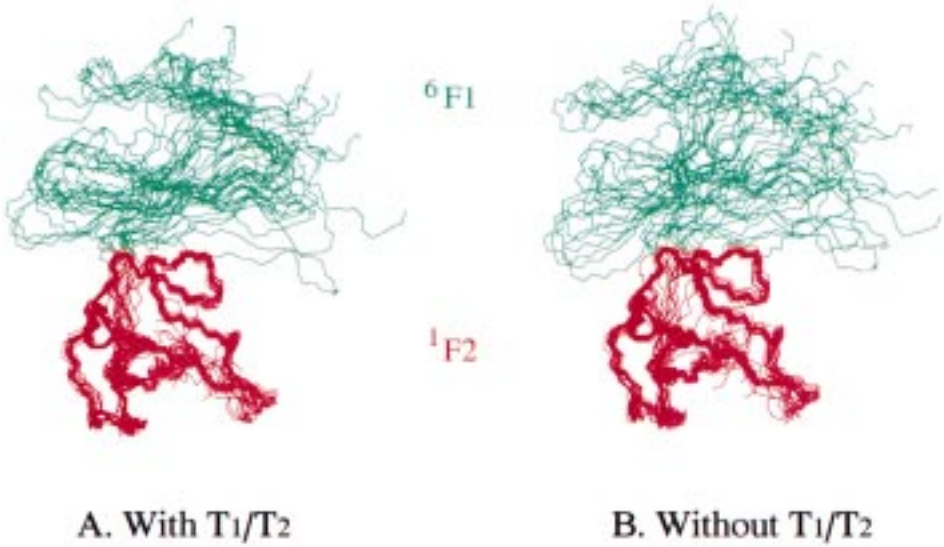

Figure 6. Effects of the T_1/T_2 restraints on structure refinement. Each subset contains 15 structures that are overlaid on the backbone heavy atoms of the ^{1}F2 module. (A) Structures were refined using T_1/T_2 restraints together with inter-module and intra-module NOEs and coupling constants. (B) Structures were refined using the same parameters and restraints as in A except for the omission of the T_1/T_2 restraints.

Evaluation of the calculated structures

Figure 6 shows the comparison of two families of 15 structures: one was calculated with T_1/T_2 restraints using the optimised parameters ($D_\parallel/D_\perp = 0.9$ and a force constant with a linear ramp between 2.0 and 3.0 kcal/mol) whereas the other was calculated without T_1/T_2 restraints. The structural statistics of the two families are presented in Table 3. As in the selection method, the inclusion of the T_1/T_2 restraints leads to a reduction of the RMSDs from 9.82 ± 4.78 Å (for the ^{1}F2 when superimposed with the ^{6}F1) and 9.27 ± 4.51 Å (for the ^{6}F1 when superimposed with the ^{1}F2) to 6.84 ± 3.79 Å and 6.64 ± 3.81 Å and a concurrent reduction of the χ^2 per residue of the T_1/T_2 ratios from 1.80 ± 0.27 to 1.42 ± 0.15. Thus, in both approaches the structural information contained in the T_1/T_2 ratios has been shown to improve the definition of the relative orientations of the two modules with respect to one another. It is important to note that the inclusion of the T_1/T_2 restraints did not introduce additional NOE violations of more than 0.3 Å and that the number of violations of more than 0.1 Å remained low. The energy difference between both families of structures is entirely due to additional E_{anis} energies in the T_1/T_2 refined structures. Hence, the total energies remain comparable to the structures calculated without T_1/T_2 restraints. In addition, the quality of the local structure was well preserved. The backbone RMSDs of the individual modules when superimposed on themselves in the presence or absence of T_1/T_2 restraints remains at about 1.1–1.3 Å and the percentage of backbone dihedral angles in the allowed regions of the Ramachandran plot also remains the same. Hence, the inclusion of the T_1/T_2 ratios improves the precision of the average module–module orientation in the ^{6}F1^{1}F2 module pair without deteriorating the structures of the individual modules.

Efficiency and limitation of the T_1/T_2 restraints

So far it has been shown that T_1/T_2 restraints are capable of improving the definition of the average relative orientation of the two modules when used in conjunction with inter-module NOE restraints. Is it possible to define the relative orientation of the two modules using T_1/T_2 restraints only? We tested the T_1/T_2 refinement without the aid of inter-module NOE restraints. The resultant structures no longer exhibited any preferential module–module orientation, as indicated by the large RMSDs of 18.81 ± 9.52 Å (for the ^{1}F2 when superimposed on the ^{6}F1) and 13.92 ± 5.53 Å (for the ^{6}F1 when superimposed on the ^{1}F2). Increasing the force constant of the T_1/T_2 restraints by a factor of 5 also did not yield any preferential structure; rather, it introduced NOE violations and high energies. Similarly, applying the selection method to this family of structures did not produce a subset of structures with a preferred orientation.

Thus, T_1/T_2 restraints by themselves are not sufficient to define uniquely the relative orientation of the two modules in the ^{6}F1^{1}F2 pair. This limitation is a result of the partial degeneracy of the main axis of the diffusion tensor and the poor sampling of the angles with respect to the unique axis. For an axially symmetric diffusion tensor the only angular information of the T_1/T_2 ratio is given relative to D_{zz} but not relative to D_{xx} or D_{yy}. In addition, poor sampling of NH bond vectors that are aligned with D_{zz} may underestimate the axial ratio of the diffusion tensor. As seen in the current example, these limitations cannot be compensated by increasing the force constants of the T_1/T_2 restraints. Hence, in our case, the structural information of T_1/T_2 ratios is best considered as a supplement to NOE and coupling constant information, rather than a source of structural information on its own.

Comparison of the selection and refinement methods

Two methods to improve the definition of the relative orientation of two modules with respect to each other have been proposed and successfully tested. A comparison of the averaged structures from the family of structures that were determined by either method showed agreement within one standard deviation. The advantage of the selection procedure is that it is simple and fast, because it only requires a non-linear fit and a subsequent ranking of the structures. However, it depends on the sampling properties of the family of initial structures. It is suitable for testing whether inclusion of T_1/T_2 ratios in a structure calculation can be expected to improve the definition of a structure. While the refinement method reduces the risk of introducing artificial bias, the optimisation of parameters and refinement protocols requires more computational time and time to analyse the results.

Conclusions

The definition of the average module–module orientation of the fibronectin ^{6}F1^{1}F2 module pair was significantly improved using the dependence of ^{15}N heteronuclear relaxation time constants on the rotational diffusion anisotropy. The relaxation data provide valuable additional long-range order information unavailable when using NOEs and coupling constants alone. Inclusion of the relaxation data yielded a significantly better defined intermodule interface without changing the structures of the individual modules. Provided a set of initial structures is available, a simple and fast method is proposed to determine whether the relaxation data contain the desired structural information. Hence, T_1/T_2 ratios are valuable and readily available sources of structural information that can be instrumental in the determination of structures of multi-domain proteins.

Acknowledgements

I.D.C., A.R.P., and J.M.W. thank the Wellcome Trust for financial support. S.P.S. is a recipient of a Burroughs Wellcome Fund Hitchings–Elion Fellowship. We would like to thank Dr. C. Redfield for providing the initial FORTRAN routine to fit the fully asymmetric diffusion tensor, Dr. K. Downing and Dr. C. Redfield for advice on T_1/T_2 structure calculations, Prof. M. Clore for providing the code for XPLOR v.3.8 including the T_1/T_2 refinement module, Dr. R. Aplin for electrospray mass spectrometry and Dr J. Boyd and N. Soffe for NMR support. This is a contribution from the Oxford Centre for Molecular Sciences that is supported by the BBSRC, MRC and EPSRC.

References

Bányai, L. and Patthy, L. (1991) *FEBS Lett.*, **282**, 23–25.

Bányai, L., Trexler, M., Koncz, S., Gyenes, M., Sipos, G. and Patthy, L. (1990) *Eur. J. Biochem.*, **193**, 801–806.

Blackledge, M., Cordier, F., Dosset, P. and Marion, D. (1998) *J. Am. Chem. Soc.*, **120**, 4538–4539.

Bocquier, A.A., Potts, J.R., Pickford, A.R. and Campbell, I.D. (1999) *Structure*, **7**, 1451–1460.

Bodenhausen, G. and Ruben, D.J. (1980) *Chem. Phys. Lett.*, **69**, 185–189.

Boyd, J., Hommel, U. and Campbell, I.D. (1990) *Chem. Phys. Lett.*, **175**, 477–482.

Boyd, J. and Redfield, C. (1998) *J. Am. Chem. Soc.*, **120**, 9692–9693.

Brünger, A.T. (1992) *X-PLOR Version 3.1. A System for X-ray Crystallography and NMR*, Yale University, New Haven, CT.

Copié, V., Tomita, Y., Akiyama, S.K., Aota, S., Yamada, K.M., Venable, R.M., Pastor, R.W., Krueger, S. and Torchia, D.A. (1998) *J. Mol. Biol.*, **277**, 663–682.

Farrow, N.A., Zhang, O., Forman-Kay, J.D. and Kay, L.E. (1994) *J. Biomol. NMR*, **4**, 727–734.

Forastieri, H. and Ingham, K.C. (1985) *J. Biol. Chem.*, **260**, 10546–10550.

Guidry, C., Miller, E.J. and Hook, M. (1990) *J. Biol. Chem.*, **265**, 19230–19236.

Hahn, L.E. and Yamada, K.M. (1979) *Proc. Natl. Acad. Sci. USA*, **76**, 1160–1163.

Hynes, R.O. (1990) In *Fibronectins* (Ed., Rich, A.), Springer-Verlag, Berlin.

Ingham, K.C., Brew, S.A. and Migliorini, M.M. (1989) *J. Biol. Chem.*, **264**, 16977–16980.

Kay, L.E., Keifer, P. and Saarinen, T. (1992a) *J. Am. Chem. Soc.*, **114**, 10663–10665.
Kay, L.E., Nicholson, L.K., Delaglio, F., Bax, A. and Torchia, D.A. (1992b) *J. Magn. Reson.*, **97**, 359–375.
Kay, L.E., Torchia, D.A. and Bax, A. (1989) *Biochemistry*, **28**, 8972–8979.
Koradi, R., Billeter, M. and Wüthrich, K. (1996) *J. Mol. Graphics*, **14**, 52–55.
Laskowski, R.A., MacArthur, M.W., Moss, D.S. and Thornton, J.M. (1993) *J. Appl. Crystallogr.*, **26**, 283–291.
Litvinovich, S.V., Strickland, D.K., Medved, L.V. and Ingham, K.C. (1991) *J. Mol. Biol.*, **217**, 563–575.
Mandel, A.M., Akke, M. and Palmer, A.G. (1995) *J. Mol. Biol.*, **246**, 144–163.
Marion, D., Ikura, M., Tschudin, R. and Bax, A. (1989) *J. Magn. Reson.*, **85**, 393–399.
Owens, R.J. and Baralle, F.E. (1986) *EMBO J.*, **5**, 2825–2830.
Palmer, A.G., Rance, N. and Wright, P.E. (1991) *J. Am. Chem. Soc.*, **113**, 4371–4380.
Phan, I.Q.H., Boyd, J. and Campbell, I.D. (1996) *J. Biomol. NMR*, **8**, 369–378.
Pickford, A.R., Potts, J.R., Bright, J.R., Phan, I. and Campbell, I.D. (1997) *Structure*, **15**, 359–370.
Potts, J.R., Bright, J.R., Bolton, D., Pickford, A.R. and Campbell, I.D. (1999) *Biochemistry*, **38**, 8304–8312.
Potts, J.R. and Campbell, I.D. (1996) *Matrix Biol.*, **15**, 313–320.
Press, W.H., Flannery, B.P., Teukolsky, S.A. and Vetterling, W.T. (1990) *Numerical Recipes*, 2nd ed., Cambridge University Press, New York, NY.
Shaka, A.J., Barker, P.B. and Freeman, R. (1985) *J. Magn. Reson.*, **64**, 547–552.
Skorstengaard, K., Holtet, T.L., Etzerodt, M. and Thøgersen, H.C. (1994) *FEBS Lett.*, **343**, 47–50.
Tjandra, N., Szabo, A. and Bax, A. (1996) *J. Am. Chem. Soc.*, **118**, 6986–6991.
Tjandra, N., Garrett, D.S., Gronenborn, A.M., Bax, A. and Clore, G.M. (1997a) *Nat. Struct. Biol.*, **4**, 443–449.
Tjandra, N., Omichinski, J.G., Gronenborn, A.M., Clore, G.M. and Bax, A. (1997b) *Nat. Struct. Biol.*, **4**, 732–738.
Tjandra, N. and Bax, A. (1997c) *Science*, **278**, 1111–1114.
Tolman, J.R., Flanagan, J.M., Kennedy, M.A. and Prestegard, J.H. (1995) *Proc. Natl. Acad. Sci. USA*, **92**, 9279–9283.
Wang, A.C. and Bax, A. (1993) *J. Biomol. NMR*, **3**, 715–720.
Williams, M.J., Phan, I., Harvey, T.S., Rostagno, A., Gold, L.I. and Campbell, I.D. (1994) *J. Mol. Biol.*, **235**, 1302–1311.
Woessner, D.E. (1962) *J. Chem. Phys.*, **36**, 1–4.
Wüthrich, K. (1986) *NMR of Proteins and Nucleic Acids*, Wiley, New York, NY.